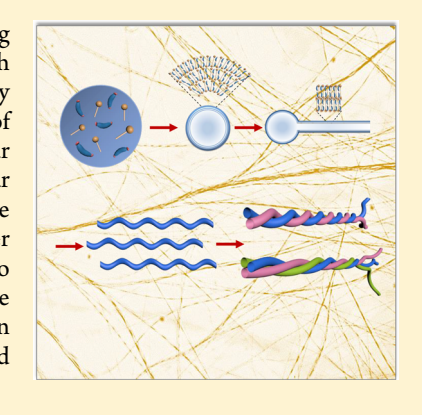
# Morphology Transformation of Supramolecular Structures in **Aqueous Mixtures of Two Oppositely Charged Amphiphiles**

Wenlang Liang,<sup>†,||</sup> Xu He,<sup>‡,§</sup> Nitin Ramesh Reddy,<sup>†</sup> Yuanli Bai,<sup>‡</sup> Linan An,<sup>†</sup> and Jiyu Fang<sup>\*,†</sup>

Supporting Information

ABSTRACT: The co-assembly of oppositely charged amphiphiles provides a fascinating approach for forming complex supramolecular structures, which are interesting from both fundamental and technological viewpoints. Here, we report a stepwise morphology transformation of co-assembled supramolecular structures in the aqueous mixture of lithocholic acid (LCA) and cetyltrimethylammonium bromide (CTAB) at mixed molar ratios of 1:1 and 2:1. The co-assembly of LCA and CTAB initially forms multilamellar vesicles followed by the spontaneous growth of membrane tubes from the vesicles. The vesicle-to-tube transition is accompanied by a fluidic-to-crystalline phase transition. After being aged, the membrane tubes twist into left-handed helices, which then intertwine into left-handed double helices and multihelix bundles. The single handedness of these supramolecular structures is a reflection of the amplification of the chirality of LCA. An understanding of the co-assembly mechanism and pathway is a key step toward producing supramolecular structures with distinguished morphologies.



## ■ INTRODUCTION

Molecular self-assembly through multiple noncovalent interactions, a ubiquitous phenomenon in nature, has emerged as a powerful strategy for forming ordered supramolecular structures at multiple length scales. 1,2 Amphiphiles are a class of relatively simple molecules that are known to self-assemble into a variety of ordered supramolecular structures with welldefined morphologies such as micelles, vesicles, fibers, ribbons, and tubes, which are of great promise for technological and medical applications.3

Bile acids are a chiral and facial amphiphile with a hydrophobic convex side and a hydrophilic concave side, which are synthesized in the liver from cholesterol and then secreted into the intestine, where they solubilize dietary lipids by forming mixed micelles.8 Besides their biological importance, the self-assembly behavior of bile acids in aqueous solution has also attracted great interest. 9,10 It was reported that bile acids could self-assemble into primary micelles through the hydrophobic interaction between their hydrophobic sides, which could further aggregate to form the secondary micelles through the hydrogen binding of primary micelles.9 The capability of these bile acid micelles for encapsulating both polar and nonpolar drugs made them suitable as drug delivery vehicles. 11,12 Recent studies also showed that bile acids and their derivatives could self-assemble into other ordered supramolecular structures such as helical ribbons, <sup>13–15</sup> nanotubes, <sup>16–18</sup> and spherulites <sup>19</sup> by controlling the condition under which the self-assembly occurred.

The co-assembly of oppositely charged amphiphiles opens a simple way to tune the morphology of supramolecular structures by modifying the balance of multiple noncovalent interactions. 20-22 It is known that the hydrophobic/hydrophilic balance of bile acids varies due to their structural diversities. Cholic acid (CA), deoxycholic acid (DCA), and lithocholic acid (LCA) are differ from each other in the number of hydroxyl groups on their steroid skeleton. The order of the hydrophobicity is LCA > DCA > CA.23 The hydrophobicity of bile acids has a significant impact on their assembly with classical amphiphiles with a flexible, hydrophobic tail and a hydrophilic head. For example, the coassembly of CA and cetyltrimethylammonium bromide (CTAB) in aqueous solution could produce spherical micelles, while the co-assembly of DCA and CTAB led to the sphericalto-cylindrical micelle transition.<sup>24</sup> Recently, the vesicle-tohelical ribbon transition was reported in the salt-free system of LCA and cetyltrimethylammonium hydroxide (CTAOH) at the equimolar ratio with the decrease of temperature. 25 In this paper, we report the co-assembly of LCA and CTAB in ammonium solution at mixed molar ratios of 1:4, 1:2, 1:1, and 2:1. The multilamellar vesicles from the co-assembly of LCA and CTAB at mixed molar ratios of 1:4 and 1:2 were found to be stable at room temperature for months, while the spontaneous growth of membrane tubes from the multilamellar

Received: April 17, 2019 Revised: May 24, 2019 Published: June 2, 2019



<sup>†</sup>Department of Materials Science and Engineering and ‡Department of Mechanical and Aerospace Engineering, University of Central Florida, Florida 32816, United States

<sup>&</sup>lt;sup>||</sup>School of Materials Science and Engineering and <sup>§</sup>School of Mechanics and Engineering, Southwest Jiaotong University, Chengdu 610031, China

vesicles formed by the co-assembly of LCA and CTAB at mixed molar ratios of 1:1 and 2:1 was observed. After being aged at room temperature, the membrane tubes twisted into left-handed helices, which further intertwined into left-handed double helices and multihelix bundles. The structure and morphology of these supramolecular structures were characterized.

### EXPERIMENTAL SECTION

**Materials.** Lithocholic acid (LCA, >98%), cetyltrimethylammonium bromide (CTAB, >99%), and ammonium solution were purchased from Sigma-Aldrich. Water used in our experiments was purified with an Easypure II system (18 M $\Omega$  cm, pH 5.7). Holey Formvar films were from SPI supplies. Si wafer was purchased from University Wafer. Glass slides and cover glass slides were from Fisher Scientific.

**Sample Preparation.** LCA was mixed with CTAB in ammonium solution at mixed molar ratios of 1:4, 1:2, 1:1, 2:1, and 4:1 in which the concentration of LCA was always kept at 1 mM. The mixed LCA/CTAB solution was sonicated at ~50 °C in an ultrasonic bath (Branson 1510, Branson Ultrasonics Co.) for 30 min and then cooled down to room temperature. After being aged in sealed glass vials, a drop of the mixed solution was placed on substrates for characterizations.

Characterization. For optical microscopy measurements, a 100  $\mu$ L drop of mixed solution was placed on a glass substrate followed by adding a cover glass slide on the top of the drop. The initial thickness of the confined vesicle solution film was estimated to be  $\sim$ 10  $\mu$ m by moving the focus plane of an optical microscope from the bottom glass substrate to the upper glass slide. Optical microscopy images were captured with a digital camera (C2020 Zoom, Olympus) mounted on an optical microscope (Olympus BX). Scanning electron microscopy (SEM) images were taken with a Zeiss Ultra-55 FEG SEM operated at 20 kV. Transmission electron microscopy (TEM) measurements were performed on a JEOL TEM-1011 operated at 100 kV. Tapping mode atomic force microscopy (AFM) images were taken by a Dimension 3100 from Veeco Instruments in which a silicon nitride cantilever (nanosensors) with a spring constant of 30 N/m and a resonant frequency of 260 kHz was used. X-ray diffraction was recorded with a Rigaku D/max diffractometer with Cu Kα radiation ( $\lambda$  = 1.542 Å) operated at 40 kV and 30 mA. Fourier transform infrared (FTIR) spectra were taken with a Perkin-Elmer (100) spectrometer operating at 4 cm<sup>-1</sup> resolution.

Numerical Simulation. The twisting behavior of membrane

**Numerical Simulation.** The twisting behavior of membrane tubes was simulated by the finite element code ABAQUS in which the membrane tubes were simulated as a neo-Hookean hyperelastic material (Method S1) with an external diameter of 1  $\mu$ m and a wall thickness of 50 nm. Shell elements were used in the simulations. During the simulation process, torque was applied to both ends of membrane tubes with varied shear moduli (Figure S1).

# ■ RESULTS AND DISCUSSION

The molecular structures of LCA and CTAB are shown in Figure 1a,b, respectively. CTAB is a cationic amphiphilic molecule with a critical micelle concentration of ~1.0 mM. LCA is a secondary bile acid with a rigid, planar steroid skeleton and a carboxyl group linked to the steroid skeleton through a short alkyl chain. The critical micelle concentration of LCA is ~1.0 mM. We found that the co-assembly of LCA and CTAB in 6% ammonia solution at mixed molar ratios of 1:4, 1:2, 1:1, and 2:1 formed microsized vesicles in which LCA concentration was kept constant (1.0 mM). Figure 1c shows an optical microscopy image of microsized vesicles formed in the mixed LCA/CTAB solution with a molar ratio of 1:1 after 30 min of aging. The high-magnification optical microscopy image of the vesicles revealed that they were multilamellar with several bilayers (Figure 1d). We also noted that the

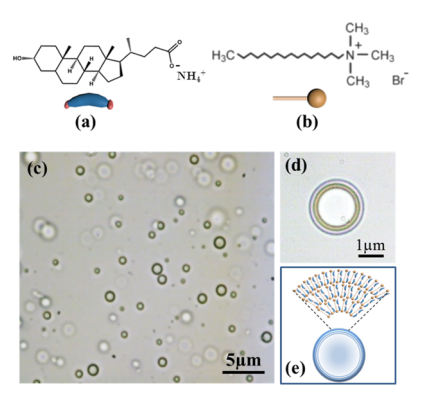


Figure 1. Chemical structure of (a) LCA and (b) CTAB. (c) Lowand (d) high-magnification optical microscopy images of mixed LCA/CTAB vesicles formed at a molar ratio of 1:1 in 6% ammonia solution. (e) Scheme of a possible arrangement of LCA and CTAB in multilamellar vesicles.

multilamellar vesicles were able to fuse into large vesicles when they collided (Figure S2), suggesting that LCA and CTAB components were in a fluidic phase.

In the absence of LCA, transmission electron microscopy (TEM) images showed the formation of micelles with a diameter of ~5 nm in 1 mM CTAB solution (Figure S3a). The observed diameter of CTAB micelles is slightly larger than that measured with dynamic light scattering in aqueous solution.<sup>26</sup> The increased diameter is likely due to the flattening of CTAB micelles after being dried on substrates for TEM measurements. In the absence of CTAB, we observed the formation of straight nanotubes with an external diameter of ~60 nm and a wall thickness of  $\sim$ 7 nm in 1 mM LCA solution (Figure S3b). The adsorption of CTAB vesicles on the external surface of LCA nanotubes was observed when 0.5 mL of vesicle solution was mixed with 5 mL of nanotube solution (Figure S3c). The controlled experiment suggests that the multilamellar vesicles shown in Figure 1c are a result of the co-assembly of LCA and CTAB. The molecular structure of LCA is significantly different from that of CTAB. The length of LCA from its hydroxyl to its carboxyl group (~1.5 nm) is shorter than that of CTAB (~2.1 nm) in a fully extended conformation. In the mixed LCA/CTAB vesicles, the hydrophobic steroidal skeleton of LCA is expected to insert into the bilayer wall of vesicles and interacts with the hydrophobic tail of CTAB (Figure 1e) in which the COO- group of LCA interacts electrostatically with the head group of CTAB.

After the mixed LCA/CTAB solution with a molar ratio of 1:1 was aged for 2 h at room temperature, membrane tubes with a diameter of  $\sim 1.0 \ \mu m$  grew from early formed vesicles (Figure 2a). They were stable without retraction even after being dried on substrates (Figure 2b). The membrane tubes showed uniform birefringence when they were viewed between two crossed polarizers (Figure 2c), suggesting that they had an extended crystalline wall (Figure 2d). It was reported that membrane tubes could be pulled from large vesicles by applying external forces. 27-30 However, the growth of membrane tubes from mixed LCA/CTAB vesicles was a spontaneous process without external forces. To elucidate the vesicle-to-tube transition mechanism in mixed LCA/CTAB solution, we changed the mixed molar ratio of LCA and CTAB and showed that there was a threshold molar ratio for the vesicle-to-tube transition. At mixed molar ratios of 1:4 and 1:2, which corresponded to lower LCA concentrations, the early

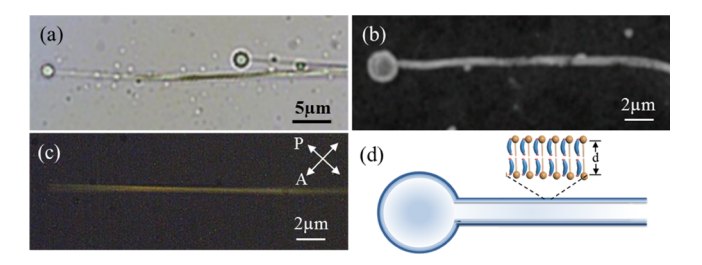
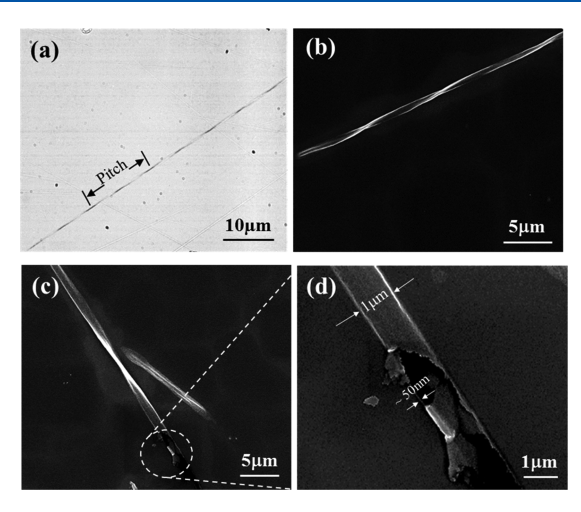


Figure 2. (a) Optical microscopy and (b) SEM images of the growth of membrane tubes from mixed LCA/CTAB vesicles formed at a molar ratio of 1:1 in 6% ammonia solution. (c) Polarizing optical image of membrane tubes. (d) Scheme of the growth of a membrane tube from a vesicle. The direction of polarizer (P) and analyzer (A) is indicated with arrows shown in (c).

formed multilamellar vesicles from the co-assembly of LCA and CTAB were stable after 1 month of aging (Figure S4a,b), while the multilamellar vesicles formed at mixed molar ratios of 1:1 and 2:1, which corresponded to higher LCA concentrations, were unstable. The spontaneous growth of membrane tubes from the vesicles formed at mixed molar ratios of 1:1 and 2:1 was observed after 2 and 1 h of aging, respectively. When the mixed molar ratio was increased to 4:1, short membrane tubes with a length of 3–4  $\mu$ m were observed within 30 min of aging (Figure S4c). The fusion of mixed LCA/CTAB vesicles shown in Figure S1 suggests that LCA and CTAB have a fluidic phase. The strong birefringence of membrane tubes indicates that LCA and CTAB form a crystalline phase. Thus, we hypothesize that the fluidic-to-crystalline (disorder-toorder) phase transition may be responsible for the vesicle-totube transition. The spontaneous growth of membrane tubes from vesicles was also reported in mixed cholesterol/ phospholipid solution with the increase of cholesterol compositions. 31,32

After 1 week of aging at room temperature, early formed vesicles at mixed molar ratios of 1:1 and 2:1 disappeared. Helical structures (single helices, double helices, and multihelix bundles) were observed (Figure S5). The closer examination with an optical microscope showed that membrane tubes periodically twisted along their long axis into helices with a pitch of  $\sim 16 \,\mu \text{m}$  (Figure 3a). SEM images revealed that helical tubes were left-handed (Figure 3b). Occasionally, we observed that helical tubes were partially broken (Figure 3c), which revealed their hollowness nature. The wall thickness of the helical tube, which was measured from the high-magnification SEM image shown in Figure 3d, was ~50 nm. X-ray diffraction revealed that the tube wall had a regular bilayer stacking with a d spacing of ~4.1 nm (Figure 4a), which is near twice the length of CTAB in its fully extended conformation (Figure 2d). Figure 4b shows the Fourier transform infrared spectrum (FTIR) of helical membrane tubes. The absorption peaks at 2850 and 2920 cm<sup>-1</sup> correspond to the stretching of the CH<sub>2</sub> in the alkyl chain of CTAB and LCA. The absorption peak at 1035 cm<sup>-1</sup> can be assigned to the stretching of the C-N of CTAB. The absorption peaks at 1550<sup>-</sup> and 1700 cm<sup>-1</sup> in the carbonyl stretching region can be assigned to the stretching vibration of the COO- and COOH groups of LCA, respectively. This result suggests the coexistence of deprotonated and protonated LCA in helical membrane tubes. The  $pK_a$  value of LCA depends on local environments. It was reported that the p $K_a$  value of LCA was  $\sim$ 7.0–8.4 in crystalline monolayers.<sup>33</sup> LCA in helical tubes should be deprotonated in



**Figure 3.** (a) Optical microscopy and (b) SEM images of a mixed LCA/CTAB helical membrane tube formed at a molar ratio of 1:1 in 6% ammonia solution after 1 week. (c) SEM image of a partially broken helical membrane tube. (d) Enlarged SEM image of the broken region of the helical membrane tube shown in (c).

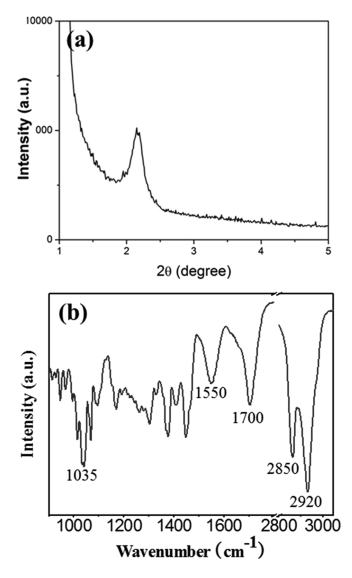


**Figure 4.** (a) X-ray diffraction and (b) FTIR spectrum of mixed LCA/CTAB helical membrane tubes formed at a molar ratio of 1:1 in 6% ammonia solution after 1 week.

ammonia solution. However, the hydrolysis of NH<sub>4</sub><sup>+</sup> may increase the acidity of the solution, which turns some of deprotonated LCA molecules to protonated LCA molecules. It was reported that the nonassociated COOH group showed an absorption peak at  $\sim 1750 \text{ cm}^{-1}$ , and the association of COOH groups through a hydrogen bond showed a peak at ~1700 cm<sup>-1</sup>.<sup>34</sup> Based on the FTIR data, we infer that the COOH group of the protonated LCA forms hydrogen bonding with the COOH or OH group of neighboring protonated LCA. The COO- group of the deprotonated LCA interacts electrostatically with the head group of CTAB in the helical membrane tubes. Mesoscale simulations showed that the shape of onedimensional supramolecular structures of chiral amphiphiles was determined by the balance between their elasticity and chirality.<sup>35</sup> The cooperation of hydrophobic interaction, hydrogen binding, and electrostatic interaction of LCA and CTAB is expected to contribute the elasticity of membrane

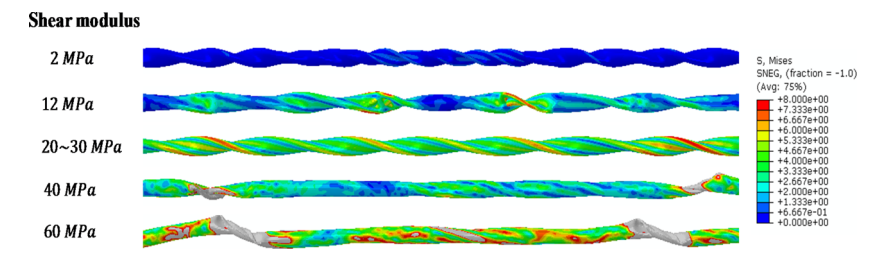
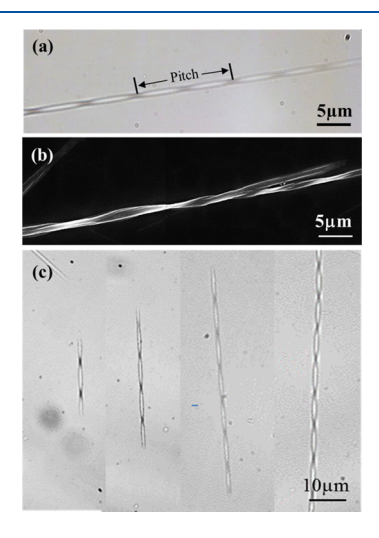


Figure 5. Simulated twisting of membrane tubes with shear moduli of 2, 12, 20–30, 40, and 60 MPa. The von Mises stress is indicated by color contours.

tubes. Our results suggest that the chiral interaction of LCA is able to provide sufficient energy to compensate for their elastic penalty to twist membrane tubes into helices.

To assess the elastic properties of membrane tubes, we simulated the twisting of membrane tubes with a diameter of 1  $\mu$ m and a wall thickness of 50 nm under torque with the finite element code ABAQUS. During the simulation process, we varied the shear modulus of membrane tubes. Figure 5 shows the twisting behavior of modeled membrane tubes with shear moduli of 2, 12, 20-30, 40, and 60 MPa. The color shown in these twisted tubes is an indication of the von Mises stress. The twisting of membrane tubes with shear moduli of 1, 12, 40, and 60 MPa under torque was localized. A uniform twisting along the long axis of membrane tubes was observed for the modeled tubes with a shear modulus of 20-30 MPa. The simulation suggests that the membrane tubes from the coassembly of LCA and CTAB have a shear modulus in this range. It was also clear from Figure 5 that the maximum stress appeared at the twisted sites where the membrane tube was significantly deformed.

Apart from single helical tubes, a significant amount of left-handed double helices was also observed. The analysis of SEM images of helical structures formed from the co-assembly of LCA and CTAB in 6% ammonia solution at a mixed molar ratio of 1:1 showed that  $\sim\!80\%$  of them was double helices. Figure 6a shows an optical microscopy image of a double helix consisting of two intertwined membrane tubes. The double



**Figure 6.** (a) Optical microscopy and (b) SEM images of mixed LCA/CTAB double helices consisting of two helical membrane tubes formed at a molar ratio of 1:1 in 6% ammonia solution after 1 week. (c) Optical microscopy images of selected double helices with a similar diameter but different lengths.

helix showed a high-fidelity braid pattern, <sup>36</sup> which originated from the 2D projection of two intertwined membrane tubes. The pitch of the double helix was  $\sim 16~\mu m$ , which is close to the pitch of the single helix shown in Figure 3a. In many cases, we observed the separation of two single helical tubes from the end of a double helical tube (Figure 6b). It was also clear from Figure 6b that both single and double helical tubes were left-handed. The same handedness reflects the amplification of the chirality of LCA in these supramolecular structures. The double helices showed a wide distribution in their lengths. However, the pitch of the double helices with the diameter remained near the same (Figure 6c).

Figure 7a shows an optical microscopy image of two double helices, which are oriented at ~35° to each other. When these

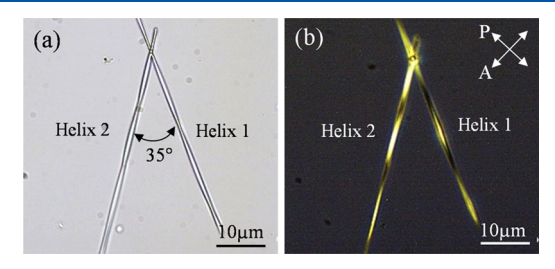
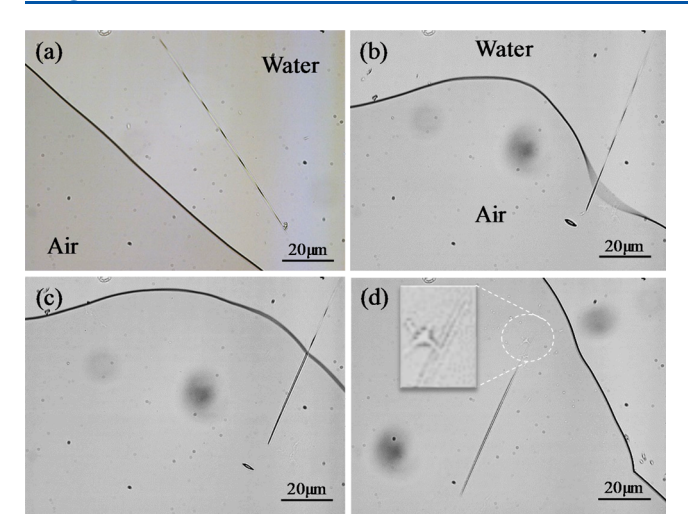


Figure 7. (a) Unpolarizing and (b) polarizing optical microscopy images of two mixed LCA/CTAB double helices formed at a molar ratio of 1:1 in 6% ammonia solution after 1 week. The direction of polarizer (P) and analyzer (A) is indicated with the arrows shown in (b).

double helices were viewed between crossed polarizer (P) and analyzer (A), they showed periodic birefringent patterns (Figure 7b). The birefringence patterns reflect the change of the crystalline direction of double helices with respect to the P direction or A direction. The double helix 1 was oriented at  $\sim 25^{\circ}$  with respect to the P direction, and the double helix 2 was oriented at  $\sim 60^{\circ}$  with respect to the P direction. The untwisted regions of the double helix 1 appeared dark in Figure 8b, suggesting that their crystalline direction was either parallel or perpendicular to the P direction, for example, at ~25° with respect to the long axis of the helix 1. The twisted regions of the double helix 2 appeared dark in Figure 8b, suggesting that their crystalline direction was either parallel or perpendicular to the P direction, for example, at 60° with respect to the long axis of the helix 2. These results also indicate that the twisting changes the crystalline direction of membrane tubes by  $\sim 35^{\circ}$ .

Occasionally, we observed the alignment of double helices by moving the air—water interface as water evaporated at room temperature. Figure 8a shows an optical microscopy image of a double helix located at the water phase of the air—water interface. The evaporation of water caused the movement of



**Figure 8.** Optical microscopy images of the moving air—water interface across a mixed LCA/CTAB double helix formed at a molar ratio of 1:1 in 6% ammonia solution. The enlarged optical microscopy image of the end of the double helix is inserted in (c).

the air-water interface in which the double helix reoriented and aligned perpendicularly with respect to the interface (Figure 8b). Interestingly, the portion of the aligned double helix in the water phase side becomes unwind. The unwinding continuously proceeded along the double helix as the airwater interface swept through it (Figure 8b,c). The inset of enlarged optical microscopy in Figure 8c shows two parallel packed tubes. The moving air-water interface of a liquid film on substrates was used to stretch coiled DNA<sup>37,38</sup> and align lipid tubes.<sup>39</sup> The technique is referred as "molecular combing". 36 In our case, the end of the double helix, which poked through the moving air-water interface, adhered on glass substrates. The surface tension of the moving air-water interface exerted a force on the double helix locally at the interface. The force (F) is proportional to the surface tension  $(\gamma)$  of the air—water interface:  $F = 2\pi d\gamma \cos \theta$ , where d is the radius of the double helix, and  $\theta$  is the contact angle of water on the double helix. In our case,  $\gamma = 72$  mN/m and  $d = \sim 0.5$  $\mu$ m.  $\theta$  is expected to be very low because the surface of double helices is hydrophilic. Thus, it is reasonable for us to assume  $\cos \theta \approx 1$ . Given these parameters, we estimated the force exerted on the double helix to be  $0.226 \times 10^{-3}$  mN, which unwound the double helix.

When 100  $\mu$ L of tube solution placed on a glass substrate was diluted by adding 50  $\mu$ L of water, we observed the separation of double helices. Figure 9a shows an optical microscopy image of a double helix, which was taken 5 s after the addition of water. The separation of the double helix from its end was observed 10 s after the addition of water (Figure 9b), which was clearly evident by the enlarged optical microscopy image inserted in Figure 9b. Two helical tubes completely separated ~20 s after the addition of water (Figure 9c). Over time, the separated helical tubes were recombined into a double helix (Figure 9d). It was reported that the intertwining of helical nanotubes into bundles could minimize their interaction energy. 40 In solution, ammonium ions are expected to screen the charge of helical membrane tubes. However, when tube solution is diluted with water, the concentration of ammonium ions decreases. Thus, the electrostatic repulsion of helical membrane tubes causes them to separate from double helices. When water evaporates,

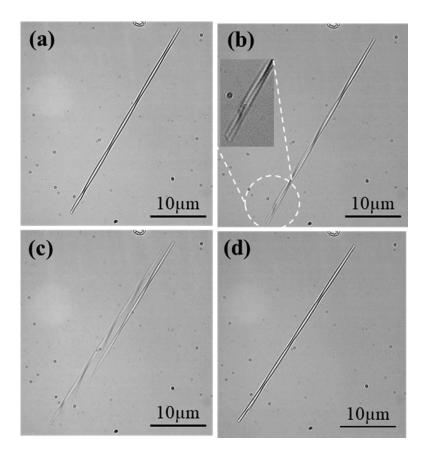


**Figure 9.** Optical microscopy images of the separation and combination of a double helix in solution. The images were taken (a) 5 s, (b) 10 s, (c) 20 s, and (d) 50 s after the addition of water. The enlarged optical microscopy image of the end of the double helix is inserted in (b).

the concentration of ammonium ions in tube solution increases. The charge of helical membrane tubes is screened by ammonium ions, which leads to the recombination of helical tubes to minimize their interaction energy.

Furthermore, we carried out the co-assembly of LCA and CTAB with a mixed ratio of 1:1 in 1% and 20% ammonia solution. The pH value of these ammonia solutions is above 11. In 1% ammonia solution, we observed the formation of vesicles, which were stable over time (Figure S6a). There was no membrane tube observed for a week. The formation of helical membrane tubes was observed in 20% ammonia solution (Figure S6b). However, they often combined to form large helical bundles with a pitch of  $\sim$ 24  $\mu$ m due to the charge screening of helical membrane tubes by ammonium ions. The small percentage of multihelix bundles was also observed in 6% ammonia solution after 1 month of aging. The multihelix bundles showed a brush-like end (Figure 10a). The enlarged optical microscopy image revealed that the intertwined range of the multihelix bundles showed a regular braid pattern with a uniform pitch of  $\sim$ 40  $\mu$ m (Figure 10b) and the brush-like end consisted of several helical tubes and double

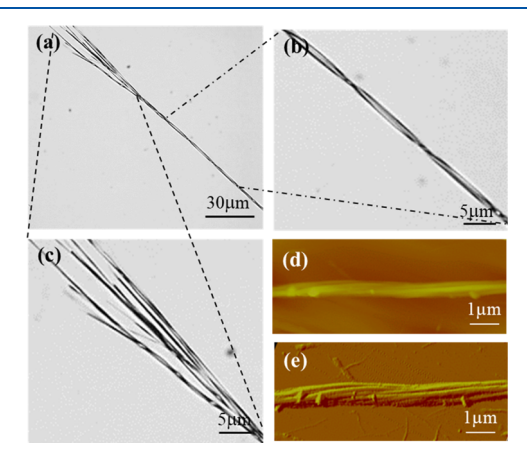


Figure 10. (a) Optical microscopy image of a multiple helix bundle in 6% ammonia solution after 1 month. Enlarged optical microscopy image of (b) intertwined range and (c) brush-like end of the multihelix bundle. (d) Topography and (e) amplitude mode AFM images of a section of a multiple helix bundle.

helices with different pitches (Figure 10c). The brush-like end is likely a result of the mismatching of the helical pitch of membrane tubes, which prevents them to intertwine. Figure 10d shows a topography mode AFM image of a section of a multihelix bundle in which individual membrane tubes in the bundle were not clearly resolved due to the tip size effect. The handedness of the multihelix bundle was better resolved in the corresponding amplitude mode AFM image, which confirmed that the bundle consisted of three left-handed helical membrane tubes (Figure 10e).

# CONCLUSIONS

We report a stepwise morphology transformation of supramolecular structures in mixed LCA/CTAB solution over time. The co-assembly of LCA and CTAB in ammonium solution at mixed molar ratios of 1:1 and 2:1 forms multilamellar vesicles followed by the spontaneous growth of membrane tubes. The vesicle-to-tube transition is accompanied by a fluidic-to-crystalline phase transition. After being aged, the membrane tubes periodically twist along their long axis into left-handed helices, which then intertwine to form left-handed double helices and multihelix bundles. The single handedness of these supramolecular structures reflects a stepwise amplification of the chirality of LCA. The helical supramolecular structures may be potentially used as templates to synthesize chiral inorganic materials.

#### ASSOCIATED CONTENT

# Supporting Information

The Supporting Information is available free of charge on the ACS Publications website at DOI: 10.1021/acs.langmuir.9b01140.

Finite element simulation of twisted tubes, photography images of mixed LCA/CTAB vesicles and twisted tubes, and TEM image of CTAB micelles and LCA nanotubes (PDF)

## AUTHOR INFORMATION

# **Corresponding Author**

\*E-mail: Jiyu.Fang@ucf.edu.

ORCID

Jiyu Fang: 0000-0002-6056-5113

Notes

The authors declare no competing financial interest.

### ACKNOWLEDGMENTS

This work was supported by the US National Science Foundation (CBET 1803690). X.H. acknowledges the financial support provided by the Chinese Scholar Council.

# REFERENCES

- (1) Lehn, J.-M. Toward Complex Matter: Supramolecular Chemistry and Self-Organization. *Proc. Natl. Acad. Sci. U. S. A.* **2002**, 99, 4763–4768.
- (2) Whitesides, G. M.; Boncheva, M. Beyond Molecules: Self-Assembly of Mesoscopic and Macroscopic Components. *Proc. Natl. Acad. Sci. U. S. A.* **2002**, 99, 4769–4774.
- (3) Shimizu, T.; Masuda, M.; Minamikawa, H. Supramolecular Nanotube Architectures Based on Amphiphilic Molecules. *Chem. Rev.* **2005**, *105*, 1401–1444.

(4) Wang, C.; Wang, Z.; Zhang, X. Amphiphilic Building Blocks for Self-Assembly: From Amphiphiles to Supra-amphiphiles. *Acc. Chem. Res.* **2012**. *45*, 608–618.

- (5) Barclay, T. G.; Constantopoulos, K.; Matisons, J. Nanotubes Self-Assembled from Amphiphilic Molecules via Helical Intermediates. *Chem. Rev.* **2014**, *114*, 10217–10291.
- (6) Liu, M.; Zhang, L.; Wang, T. Supramolecular Chirality in Self-Assembled Systems. *Chem. Rev.* **2015**, *115*, 7304–7397.
- (7) Hendricks, M. P.; Sato, K.; Palmer, L. C.; Stupp, S. I. Supramolecular Assembly of Peptide Amphiphiles. *Acc. Chem. Res.* **2017**, *50*, 2440–2448.
- (8) Maldonado-Valderrama, J.; Wilde, P.; Macierzanka, A.; Mackie, A. The role of Bile Salts in Digestion. *Adv. Colloid Interface Sci.* **2011**, 165, 36–46.
- (9) Madenci, D.; Egelhaaf, S. U. Self-Assembly in Aqueous Bile Salt Solutions. *Curr. Opin. Colloid Interface Sci.* **2010**, *15*, 109–115.
- (10) di Gregorio, M. C.; Travaglini, L.; Del Giudice, A.; Cautela, J.; Pavel, N. V.; Galantini, L. Bile Salts: Natural Surfactants and Precursors of a Broad Family of Complex Amphiphiles. *Langmuir* **2019**, 6803.
- (11) Li, R.; Carpentier, E.; Newell, E. D.; Olague, L. M.; Heafey, E.; Yihwa, C.; Bohne, C. Effect of the Structure of Bile Salt Aggregates on the Binding of Aromatic Guests and the Accessibility of Anions. *Langmuir* **2009**, *25*, 13800–13808.
- (12) Nurunnabi, M.; Khatun, Z.; Revuri, V.; Nafiujjaman, M.; Cha, S.; Cho, S.; Huh, K. M.; Lee, Y.-k. Design and Strategies for Bile Acid Mediated Therapy and Imaging. *RSC Adv.* **2016**, *6*, 73986–74002.
- (13) Blow, D. M.; Rich, A. Studies on the Formation of Helical Deoxycholate Complexes. J. Am. Chem. Soc. 1960, 82, 3566–3571.
- (14) Qiao, Y.; Lin, Y.; Wang, Y.; Yang, Z.; Liu, J.; Zhou, J.; Yan, Y.; Huang, J. Metal-Driven Hierarchical Self-Assembled One-Dimensional Nanohelices. *Nano Lett.* **2009**, *9*, 4500–4504.
- (15) Terech, P.; Velu, S. K. P.; Pernot, P.; Wiegart, L. Salt Effects in the Formation of Self-Assembled Lithocholate Helical Ribbons and Tubes. J. Phys. Chem. B 2012, 116, 11344–11355.
- (16) Terech, P.; Talmon, Y. Aqueous Suspensions of Steroid Nanotubules: Structural and Rheological Characterizations. *Langmuir* **2002**, *18*, 7240–7244.
- (17) Soto Tellini, V. H.; Jover, A.; Meijide, F.; Vázques Tato, J.; Galantini, L.; Pavel, N. V. Supramolecular Structures Generated by a p-tert-Butylphenyl-amide Derivative of Cholic Acid: From Vesicles to Molecular Tubes. *Adv. Mater.* **2007**, *19*, 1752–1756.
- (18) Zhang, X.; Bera, T.; Liang, W.; Fang, J. Longitudinal Zipping/Unzipping of Self-Assembled Organic Tubes. *J. Phys. Chem. B* **2011**, 115, 14445—14449.
- (19) Tamhane, K.; Zhang, X.; Zou, J.; Fang, J. Assembly and Disassembly of Tubular Spherulites. *Soft Matter* **2010**, *6*, 1224–1228.
- (20) Kaler, E. W.; Murthy, A. K.; Rodriguez, B. E.; Zasadzinski, J. A. Spontaneous Vesicle Formation in Aqueous Mixtures of single-tailed surfactants. *Science* **1989**, *245*, 1371–1374.
- (21) Zemb, T.; Dubois, M.; Demé, B.; Gulik-Krzywicki, T. Self-Assembly of Flat Nanodiscs in Salt-Free Catanionic Surfactant Solutions. *Science* **1999**, 283, 816–819.
- (22) Cui, H.; Hodgdon, T. K.; Kaler, E. W.; Abezgauz, L.; Danino, D.; Lubovsky, M.; Talmon, Y.; Pochan, D. J. Elucidating the Assembled Structure of Amphiphiles in Solution Via Cryogenic Transmission Electron Microscopy. *Soft Matter* **2007**, *3*, 945–955.
- (23) Griffiths, W. J.; Sjövall, J. Bile Acids: Analysis in Biological Fluids and Tissues. *J. Lipid Res.* **2010**, *51*, 23–41.
- (24) Swanson-Vethamuthu, M.; Almgren, M.; Karlsson, G.; Bahadur, P. Effect of Sodium Chloride and Varied Alkyl Chain Length on Aqueous Cationic Surfactant—Bile Salt Systems. Cryo-TEM and Fluorescence Quenching Studies. *Langmuir* 1996, 12, 2173—2185.
- (25) Liu, C.; Cui, J.; Song, A.; Hao, J. A Bile Acid-Induced Aggregation Transition and Rheological Properties in Its mixtures with Alkyltrimethylammonium Hydroxide. *Soft Matter* **2011**, *7*, 8952–896.
- (26) Dorshow, R.; Briggs, J.; Bunton, C. A.; Nicoli, D. F. Dynamic Light Scattering from cetyltrimethylammonium Bromide micelles.

Intermicellar Interactions at Low Ionic Strengths. *J. Phys. Chem.* **1982**, 86, 2388–2395.

- (27) Karlsson, A.; Karlsson, R.; Karlsson, M.; Cans, A.-S.; Strömberg, A.; Ryttsén, F.; Orwar, O. Networks of Nanotubes and Containers. *Nature* **2001**, 409, 150–152.
- (28) Rossier, O.; Cuvelier, D.; Borghi, N.; Puech, P. H.; Derényi, I.; Buguin, A.; Nassoy, P.; Brochard-Wyart, F. Giant Vesicles under Flows: Extrusion and Retraction of Tubes. *Langmuir* **2003**, *19*, 575–584.
- (29) West, J.; Manz, A.; Dittrich, P. S. Lipid Nanotubule Fabrication by Microfluidic Tweezing. *Langmuir* **2008**, *24*, *6754–6758*.
- (30) Tan, Y.-C.; Shen, A. Q.; Li, Y.; Elson, E.; Ma, L. Engineering Lipid Tubules Using Nano-Sized Building Blocks: The Combinatorial Self-Assembly of Vesicles. *Lab Chip* **2008**, *8*, 339–345.
- (31) Nomura, S.-i. M.; Mizutani, Y.; Kurita, K.; Watanabe, A.; Akiyoshi, K. Changes in the Morphology of Cell-Size Liposomes in the Presence of Cholesterol: Formation of Neuron-like Tubes and Liposome Networks. *Biochim. Biophys. Acta* **2005**, *1669*, 164–169.
- (32) Mui, B. L.; Döbereiner, H. G.; Madden, T. D.; Cullis, P. R. Influence of Transbilayer Area Asymmetry on the Morphology of Large Unilamellar Vesicles. *Biophys. J.* **1995**, *69*, 930–941.
- (33) Leonard, M. R.; Bogle, M. A.; Carey, M. C.; Donovan, J. M. Spread Monomolecular Films of Monohydroxy Bile Acids and Their Salts: Influence of Hydroxyl Position, Bulk pH, and Association with Phosphatidylcholine. *Biochemistry* **2000**, *39*, 16064–16074.
- (34) Lichkus, A. M.; Painter, P. C.; Coleman, M. M. Hydrogen Bonding in Polymer Blends. 5. Blends Involving Polymers Containing Methacrylic Acid and Oxazoline Groups. *Macromolecules* **1988**, *21*, 2636–2641.
- (35) Selinger, R. L. B.; Selinger, J. V.; Malanoski, A. P.; Schnur, J. M. Shape Selection in Chiral Self-Assembly. *Phys. Rev. Lett.* **2004**, *93*, 158103
- (36) Artin, E. Theory of braids. Ann. Math. 1947, 48, 101-126.
- (37) Bensimon, A.; Simon, A.; Chiffaudel, A.; Croquette, V.; Heslot, F.; Bensimon, D. Alignment and Sensitive Detection of DNA by a Moving Interface. *Science* **1994**, *265*, 2096–2098.
- (38) Jing, J.; Reed, J.; Huang, J.; Hu, X.; Clarke, V.; Edington, J.; Housman, D.; Anantharaman, T. S.; Huff, E. J.; Mishra, B.; Porter, B.; Shenker, A.; Wolfson, E.; Hiort, C.; Kantor, R.; Aston, C.; Schwartz, D. C. Automated High Resolution Optical Mapping Using Arrayed, Fluid-Fixed DNA Molecules. *Proc. Natl. Acad. Sci. U. S. A.* 1998, 95, 8046–8051.
- (39) Zhao, Y.; Fang, J. Positioning and Alignment of Lipid Tubules on Patterned Au Substrates. *Langmuir* **2006**, *22*, 1891–1895.
- (40) Teich, D.; Fthenakis, Z. G.; Seifert, G.; Tománek, D. Nanomechanical Energy Storage in Twisted Nanotube Ropes. *Phys. Rev. Lett.* **2012**, *109*, 255501.